Microfractographic characteristics and fracture toughness of 7000 and 2000 series aluminium alloys: proposal of a static fracture model

E. DI RUSSO, Aluminia S.p.A., Istituto Sperimentale dei Metalli Leggeri, Novara, Italy.

Abstract

The results of SEM examinations performed on fracture surfaces of CT test pieces used for determining the toughness index K_{Ic} of five high strength aluminium alloys of 7000 and 2000 series, were correlated with the fracture toughness data obtained on such alloys. A relation was formulated, in a form suggested by fracture mechanics, which links the average width of the stretched zone of the five alloys with their K_{Ic} values. Moreover, a static fracture model was proposed, which reasonably explains the micromechanisms underlaying the formation of the cliff, that is the sharp discontinuity (step) joining the stretched zone to the overload fracture region.

Riassunto

Caratteristiche microfrattografiche e tenacità alla frattura di leghe complesse 7000 e 2000: proposta di un modello di frattura statica

I risultati di esami condotti al SEM su superfici di frattura di provette CT impiegate per la determinazione dell'indice K_{Ic} di cinque leghe d'alluminio ad elevata resistenza meccanica dei gruppi 7000 e 2000, sono stati correlati con i dati di tenacità alla frattura rilevati su dette leghe.
È stata formulata una relazione, in una forma suggerita dalla meccanica della frattura, che lega la larghezza media della " stretched zone " (zona deformata all'apice della cricca di fatica) con i valori di K_{Ic}.
È stato inoltre proposto un modello di frattura statica che interpreta ragionevolmente i micromeccanismi che sono alla base della formazione del " cliff " (sbalzo), cioè della discontinuità a gradino, che unisce la " stretched zone " alla regione rotta per sovraccarico.

Introduction

Understanding of the mechanism of crack propagation in a metallic material can be aided by investigation of those characteristics of the fracture surfaces that can be correlated with an alloy's fracture toughness and possibly its microstructure.
Even a rough measurement of those characteristics can be useful when analysing fractures that occur in service, because the values of K_{Ic} and the stresses at failure can be estimated from it if they are not obtainable in another way.
This paper refers to the results of SEM observations of the fracture surfaces of compact-tension (CT) testpieces used for determining the toughness index K_{Ic} of four Al-Zn-Mg-Cu 7000-series and one Al-Cu-Mg 2000-series high-strength aluminium alloys: Aluminium Association 7012, 7010A, 7475, 7050, and 2124 (1).
The observations resulted in the determination of the average amplitude of the " stretched zone ", or transition strain zone, between the fatigue-precracked region and the region ruptured by overloading of the fracture surface. The values were correlated with the fracture toughness data, and this correlation has been given an analytic form.
On the basis of what was found in the experimental investigations a static fracture model was proposed which is capable of explaining the special fractographic features observed on the CT testpieces, and in particular the presence of a discontinuity or " cliff " joining the stretched zone to the region ruptured by overloading.

Earlier works

The literature contains many attempts to interpret the microfractographic observations made by electron microscope, to correlate what these can tell about fracture morphology with the values that can be found from mechanical testing.
For these purposes the most significant parameter is the critical value of the factor K; using that factor it is possible to assess the mechanisms that operate to initiate an unstable fracture, which are the subject of the observations by electron microscope.
It was observed in particular, on the testpieces used for determining K_{Ic}, that there was a transition zone between the fatigue-precracked region and the region of unstable crack propagation; this was called the stretched zone (SZ).
In appearance, the SZ is a surface with no special features, or with wide undulations that are easy to distinguish from the fatigue striations of the adjacent region.
Spitzig (2) considers it reasonable to assume that the SZ corresponds to the region where the crack extends through the plastic zone at the fatigue crack's tip at the instant that fast overload rupture begins.
In addition, after noting that the amplitude W of that zone increases with increasing fracture toughness, he found that the amplitude agreed well with the dimensions of the process zone — the zone of tensile instability at the crack tip according to Krafft's model (3,4) — and bore a relationship to the crack tip opening displacement (CTOD).
More specifically (5), Spitzig puts W d_T, where d_T is the distance from the crack tip according to Krafft, and establishes the following correlation between the SZ width W and K_{Ic}:

$$W = \frac{K_{Ic}^2}{2\,E\,\sigma_{ys}}$$

(σ_{ys} = yield strength; E = Young's modulus).

Other authors have made systematic measurements of the width of the SZ, both on steels and on aluminium alloys. Bates et al. (6) succeeded in making a quantitative correlation of the width with the fracture toughness index by means of the following equation:

$$\text{SZ width (inches)} = 9.2 \times 10^{-4} \left(\frac{K_{Ic}}{\sigma_{ys}}\right)^{1.7}$$

whereas Otsuka et al. (7) propose the following relation:

$$W = b\left(\frac{K_{Ic}}{\sigma_{ys}}\right)^2 - C$$

(b and C are constants).

According to Gerberich and Hemmings (8), the SZ width might be influenced by the operation of fatigue precracking, particularly if this is done with too high a load.
In a work on Al-Zn-Mg alloys by Broek (9), the SZ is held to be the result of crack tip blunting, deriving from plastic slip phenomena due to the intense stress field in front of the actual crack.
The SZ's characteristic undulations are evident signs of this slip. The crack tip blunting also determines the CTOD, which is why Broek correlates the SZ depth d with the CTOD (specifically, CTOD = 2d), regarding this dimension as more significant than the width W.
Broek comes to the following conclusions:
– The most important SZ parameter associated with K_{Ic} is probably the SZ's depth d rather than its width W.
– There appears to be a correlation between d and W: W = 1.4d.
– There is the following correlation between d and K_{Ic}:

$$2d = 0.4\frac{K_{Ic}^2}{E\,\sigma_{ys}}$$

Krasowsky and Vainshtok (10) also made depth measurements of the SZ on ductile steels and describe its form on the basis of the ratio W/d, depending on temperature and the strain-stress condition at the crack tip. They consider that SZ depth can be better linked with fracture toughness than with W.
To formulate a correlation between SZ width and K_{Ic} in a heat treating steel, Sarracino and Venzi (11) resort to analytic representations (like Bates et al. in their work), and particularly that proposed by McClintock and Irwin (12) for the radius r_p of the plastic zone at the bottom of the notch, which in plane strain conditions is defined as:

$$r_p = \frac{1}{6\pi}\left(\frac{K_{Ic}}{\sigma_{ys}}\right)^2$$

This procedure is justified by the fact that, whatever may be the physical interpretation of the existence of the SZ, it is without doubt strongly linked to the dimensions of the plastic zone at the crack tip.
The cited authors arrive at the following equation:

$$\frac{K_{Q^2}}{\sigma_{ys}} = 3.160\, W_{SZ}^{\;0.255}$$

with a correlation coefficient of 0.92.
More recently, Firrao and Roberti (13-15) investigated low-carbon steels with the aim of establishing a correlation between microstructure parameters and fracture toughness (K_{Ic} or J_{Ic}). Their research led to the definition of a new ductile fracture nucleation model that takes account of the increase in root radius of a crack before it is the source of rupture.
This (critical) radius would appear to be of the same order of magnitude as the spacing between the non-metallic inclusions of larger diameter. The model was used as a basis for equations by which the values of K_{Ic} or J_{Ic} can be computed, starting from the average spacing of the non-metallic inclusions and other characteristic parameters of the material under investigation.
Another fractographic feature whose dimensions have been related to toughness values is the "cliff" or overhang that links the SZ to the region ruptured by overload.
First revealed by Peel et al. (16), it links the tip of the

TABLE 1 - Actual chemical composition of alloys 7012, 7010A, 7050, 7475 and 2124

Alloy	Zn %	Mg %	Cu %	Cr %	Zr %	Mn %	Ti %	Fe %	Si %
7012	6.31	2.05	0.95	—	0.10	0.10	0.069	0.072	0.045
7010A	6.32	2.37	1.78	—	0.13	0.10	0.069	0.085	0.060
7050	6.33	2.38	2.38	—	0.10	—	0.03	0.073	0.037
7475	5.94	2.52	1.78	0.21	—	—	0.055	0.110	0.033
2124	—	1.60	4.49	—	—	0.60	0.033	0.10	0.037

fatigue crack, or more correctly the tip of the SZ, with the nearest "weak" plane fractured by overload, which might be a plane with concentrations of intermetallic compounds, or a grain boundary.
No hypothesis interpreting the particular orientation of the cliff (90°) in relation to the direction of crack propagation is stated.
In earlier ISML works on 7000-series alloys (17,18) measurements were made of the SZ width and the cliff height, resulting in the following relation:

$$h \text{ (cliff height in } \mu m) = 2.8 \left(\frac{K_{Ic}}{\sigma_{ys}}\right)^2$$

It was qualitatively confirmed in this work also that SZ width increases with increasing K_{Ic}.

Materials used

The investigations covered five of the latest aluminium alloys of the 7000 and 2000 series used in aircraft structures (7012, 7010A, 7050, 7475 and 2124 - see Table 1).
They were produced as flat forgings, of thickness 55 mm, from ingots obtained by water chill casting. The basic working cycles were the same for the various alloys, in order to secure the most meaningful possible comparison between the different materials' mechanical properties, particularly the fracture toughness characteristics, which of course are closely linked to many structural parameters (grain size, recrystallization state, extent of plastic transformation provided and degree of directionality of the semi-wrought product, density and dimensional development of the intermetallic compounds, precipitation-hardening structure).
Figures 1-3 show the microstructures of the forgings after solution treatment at the temperatures normally used by producers (for alloys 7012, 7010A and 7050 - 477-480°C; 7475 - 468-471°C; 2124 - 494-497°C) for 3-4 hours at steady state, quenching in water at 20-25°C, cold straining at 2% for the 7000 alloys and 3% for the 2124 alloy, two-stage aging for the 7000 alloys (7012 and 7010A - 106-108°C for 8 hours and 165-167°C for 24 hours; 7050 - 120-122°C for 24 hours and 176-178°C for 8 hours; 7475 - 106-108°C for 8 hours and 176-178°C for 8 hours (T73 cycles), and constant-temperature aging (190-192°C for 12 hours) for the 2124 alloy (T8 cycle).
The forgings show marked directionality of the granular aggregate in the direction of prevalent deformation (Fig. 1). No significant differences are noted in the size of the "grains" between one forging and another, whose granular structures appeared to be of mixed type, consisting of subgrain aggregates ("grains") and scattered recrystallized grains (Fig. 2).
In the 2124 alloy the recrystallized grains are found to

Fig. 1 - Grain structures of alloys taken on section S-L. The forgings show marked directionality of the granular aggregate in the direction of prevailing deformation. Etched with 2% HF anodic reagent, (× 50).

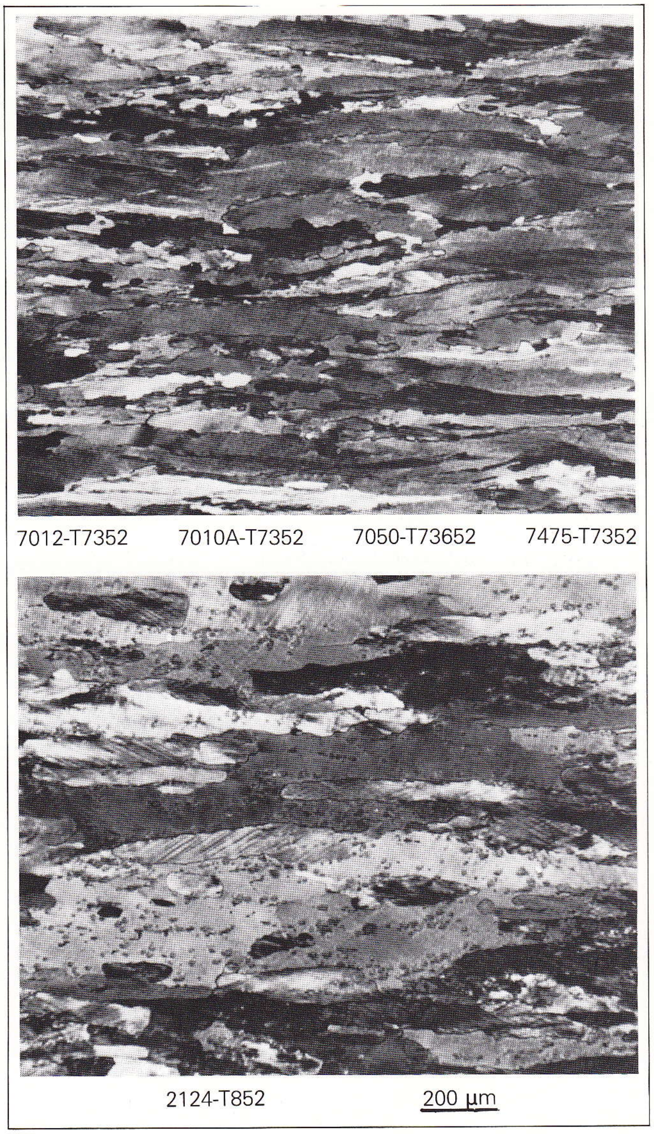

Fig. 2 - Typical forging grain structure (section S-L), consisting of subgrains and scattered recrystallized grains. Etched with 25% HNO_3 solution at about 70°C, (× 500).

Fig. 3 - Microstructures of forgings etched with selective reagent. Section T-L at about mid thickness. Etched in 0.5% HF solution, (× 100).

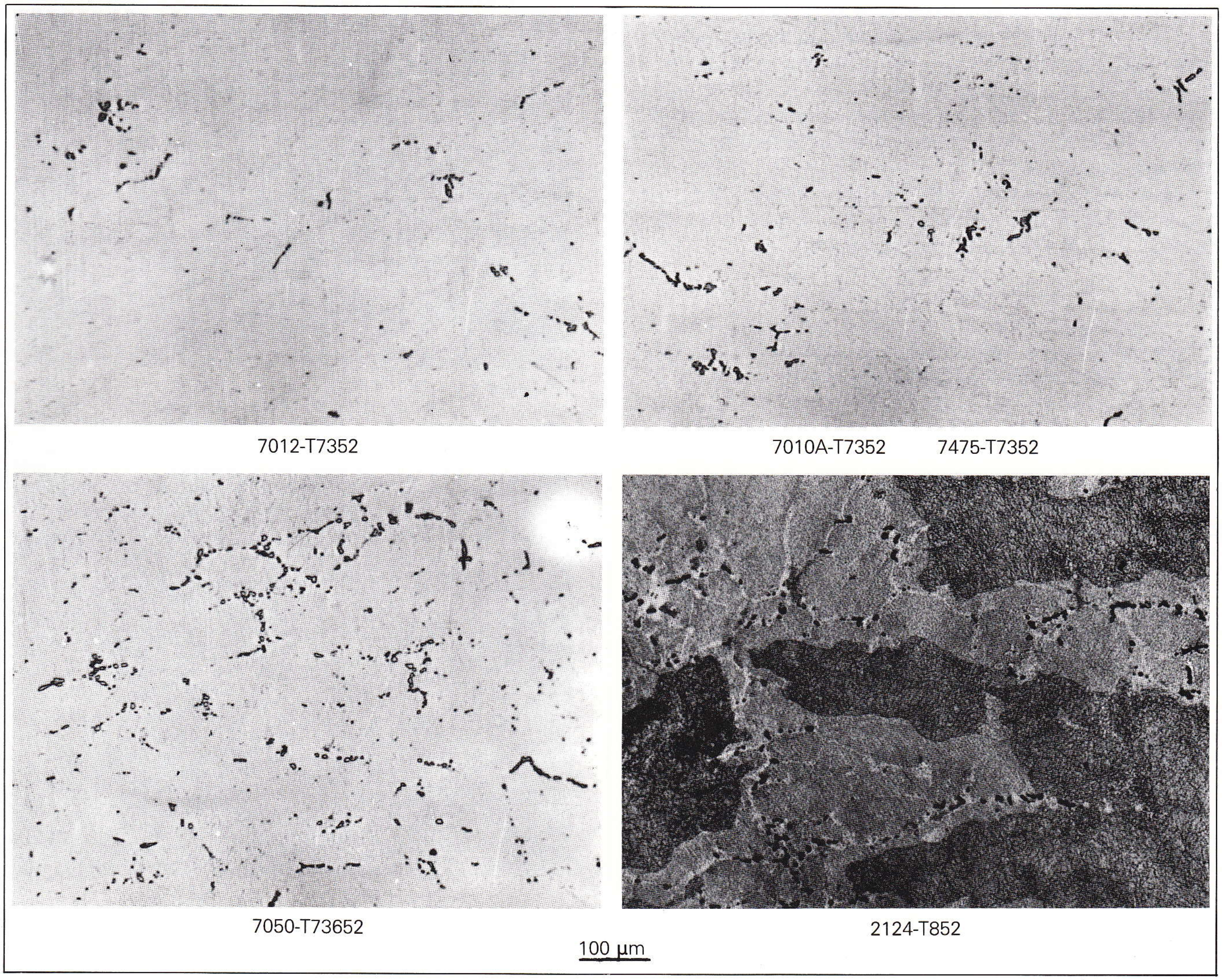

be somewhat more developed, and more numerous. In regard to the 7000 alloys, however, appreciable differences were found in the amount of secondary phases, whose numbers steadily increase from alloy 7012 to 7010A and particularly to 7050; in this respect alloy 7475 is comparable to 7010A (Fig. 3).
The secondary phases in alloys 7012, 7010A and 7475 are mainly **α** (Al Fe Si), Al_7Cu_2Fe and, to a very small extent, Mg_2Si; in alloy 7050, in addition to these compounds, there are numerous globular crystals of a phase containing Cu (Fig. 2), which cannot be eliminated even after solution treatment at high temperatures.
In alloy 2124 many crystals of phases containing Cu (+ Mg) and Mn (+ Fe + Si) remain after solution treatment (Fig. 3).
Table 2 gives the results of tensile tests (S direction) on smooth and notched ($K_t = 10.8$) round test pieces and fracture toughness tests (crack orientation S-L) to ASTM E-399-74.
Study of them reveals the following:

— 7012 has a very slightly lower YS than 7475, but has higher ductility, notch toughness NTS/YS and fracture toughness (K_{Ic}).
— 7475 has better ductility and toughness than 2124, 7050 and 7010A.
— 7050, with an YS only about 13 N/mm^2 higher, has lower ductility and, in particular, lower NTS/YS and K_{Ic} than 7010A.
— 2124 has lower ductility and toughness than all the 7000 alloys.

TABLE 2 - Average values of the mechanical properties of forgings of alloys 7012, 7010A, 7050, 7475 and 2124 in the short transverse direction (S)

Alloys	TS N/mm^2	YS at 0.2% offset N/mm^2	E %	RA %	NTS ($K_t = 10,8$) N/mm^2	$\frac{NTS}{YS}$	(*) K_{Ic} $MN \cdot m^{-\frac{3}{2}}$	$N \cdot mm^{-\frac{3}{2}}$
7012 - T7352	490	417	7.6	22.6	632	1.50	31.1	985
7010A - T7352	549	471	4.5	9.5	564	1.20	24.8	786
7050 - T73652	561	484	4.2	9.3	523	1.08	22.4	707
7475 - T7352	515	428	5.5	10.9	581	1.35	27.5	871
2124 - T852	501	461	3.1	6.4	334	0.73	19.8	628

(*) Crack orientation S-L - the first letter indicates the loading direction and the second the crack propagation direction.
S = short transverse direction and
L = longitudinal direction.

Fig. 4 - Area examined in the CT testpieces used for the fracture toughness tests, comprising the transition zone between fatigue fracture and overload fracture, excluding outer edges.

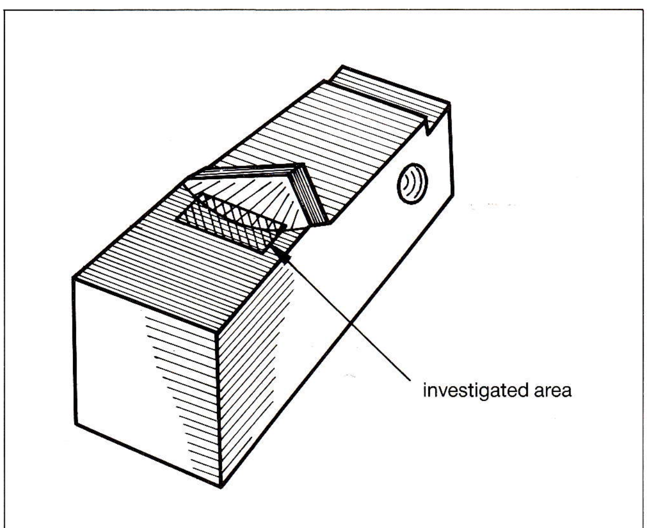

Examination with scanning microscope

The CT testpieces were examined by scanning microscope in the region shown in Fig. 4, covering the transition zone between fatigue fracture and overload fracture, excluding the outer edges.
The testpieces were sputtered with a thin layer (30 nm) of gold to give a sharper image.
The microfractographs in Fig. 5-9 are examples of the surface morphology in the transition region between fatigue precrack and overload fracture.
In the SZ, indicated in Fig. 5 by the letter S (with the fatigue-fractured zone indicated by F), can be seen the wide undulations testifying to the slip processes that generated it.

Fig. 5 - Details of fracture surface of CT testpieces of alloy 7012, showing the transition region between the fatigue zone and the overload zone.
F = fatigue fracture zone
O = overload zone
S = stretched zone
C = cliff
The fractures can be explained partly as case (A) of the diagrams in Figs. 10 and 11.

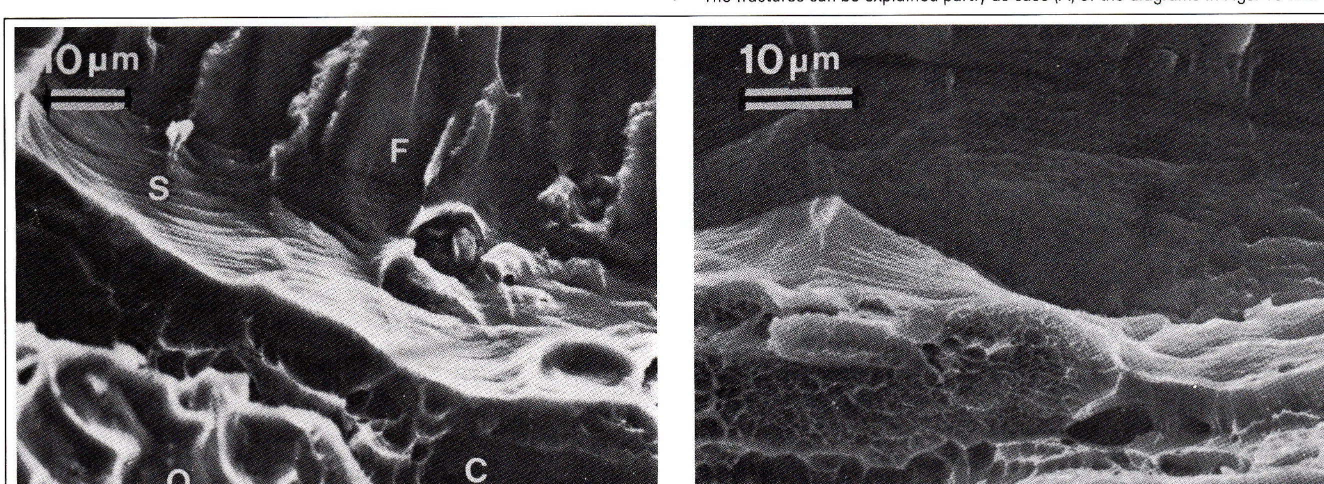

a) b)

Then there is the cliff (C), whose plane has an orientation of about 90° to the overload fracture region (O).
The latter appears " covered " in part by wide cavities (dimples) originating from secondary phase particles, and in part by microdimples nucleated from dispersoids and transition phases. Inside some of the dimples the particles that nucleated them can be seen.
Study of the fracture surfaces for all the alloys also reveals other distinguishing features of the fatigue-overload transition zone, particularly the typical aspect of the cliff covered with microdimples (see Fig. 5b and 8a, for example), which is often discontinuous in adjacent positions of the crack's leading edge; it appears sometimes to rise, and sometimes to descend, towards the overload fracture plane, and sometimes it does not appear at all (Fig. 6b, 7a and 9b).
The cliff's height tends to be greater in the tougher

Fig. 6 - Transition region in alloy 7010A. The micrographs represent cases (A) and (B) respectively.

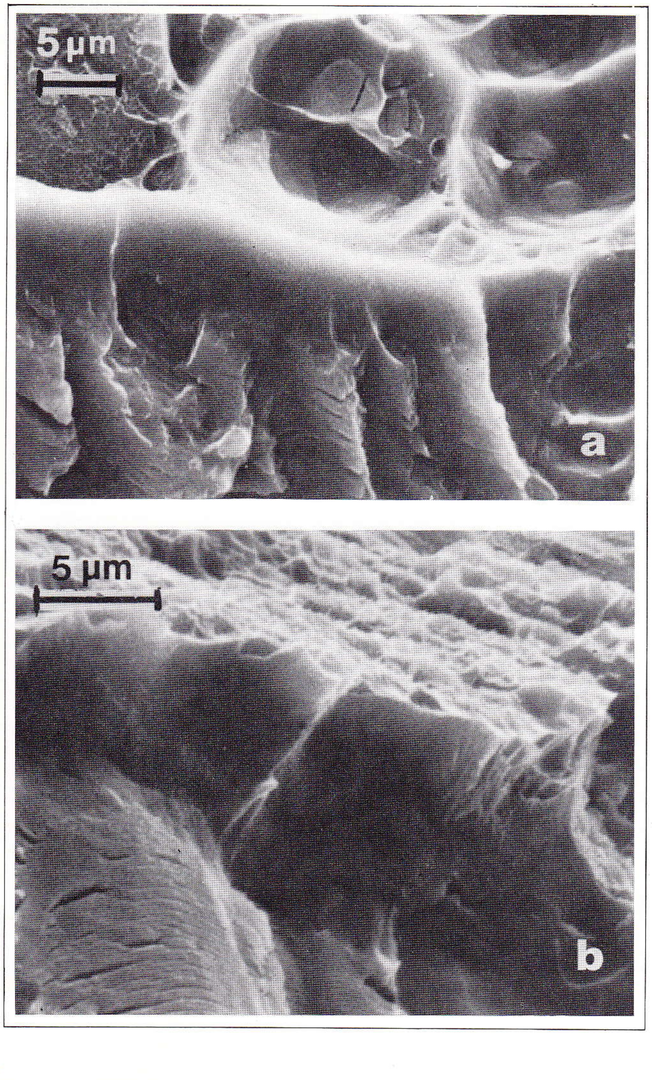

Fig. 7 - Transition region in alloy 7050. Note how the front of fracture advance is not always uniform; this phenomenon is accentuated for the less tough alloys. Cases (A) and (D).

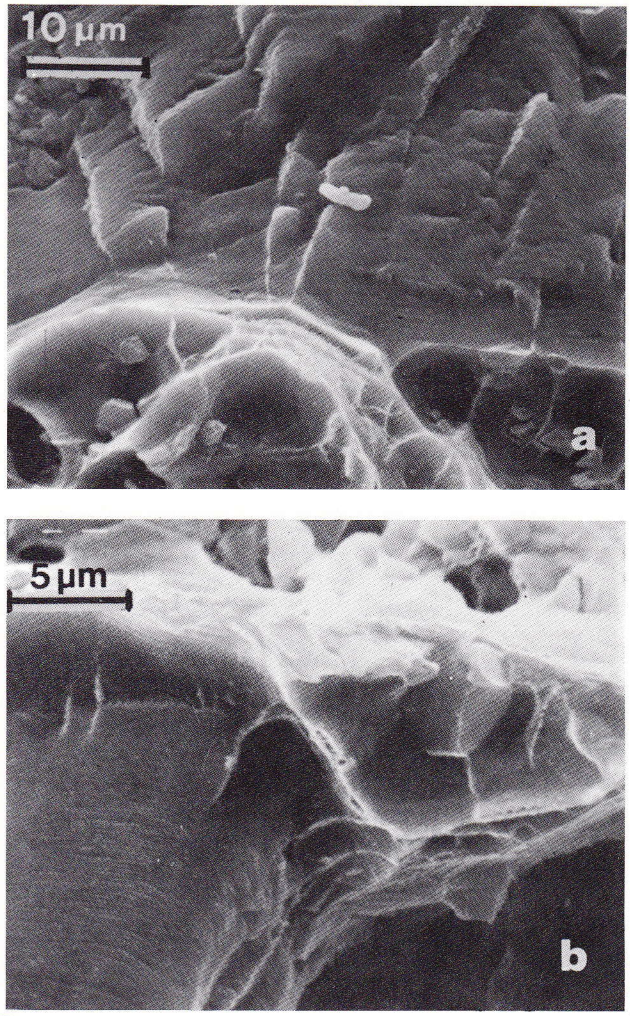

alloys, which agrees with the findings of our earlier investigations.
The SZ may also be absent, especially in the less tough alloys (7050 and 2124). In these the fracture's leading edge is not always uniform, and near the transition region there may be strong similarities in appearance between the fatigue zone and the overload fracture zone.
The observations made by SEM have been shown schematically in Fig. 10 and 11 as four typical cases of initiation of unstable crack propagation.
Case A (Fig. 10) - Possibly the commonest situation. From left to right it shows the fatigue crack F, the stretched zone S, the microdimpled cliff C, and the overload fracture O with generally much bigger dimples.
Case B (Fig. 10) - The crack continues to propagate in the same propagation plane as the fatigue precrack, but first traverses a zone of microdimples of similar size to those found on the cliff walls, or slightly larger.

Fig. 8 - Transition region in alloy 7475. The fracture surfaces are explainable as cases (A) and (C) respectively. Fig. 8a clearly shows the fractographic details characteristic of the fatigue zone, SZ, cliff, and overload zone.

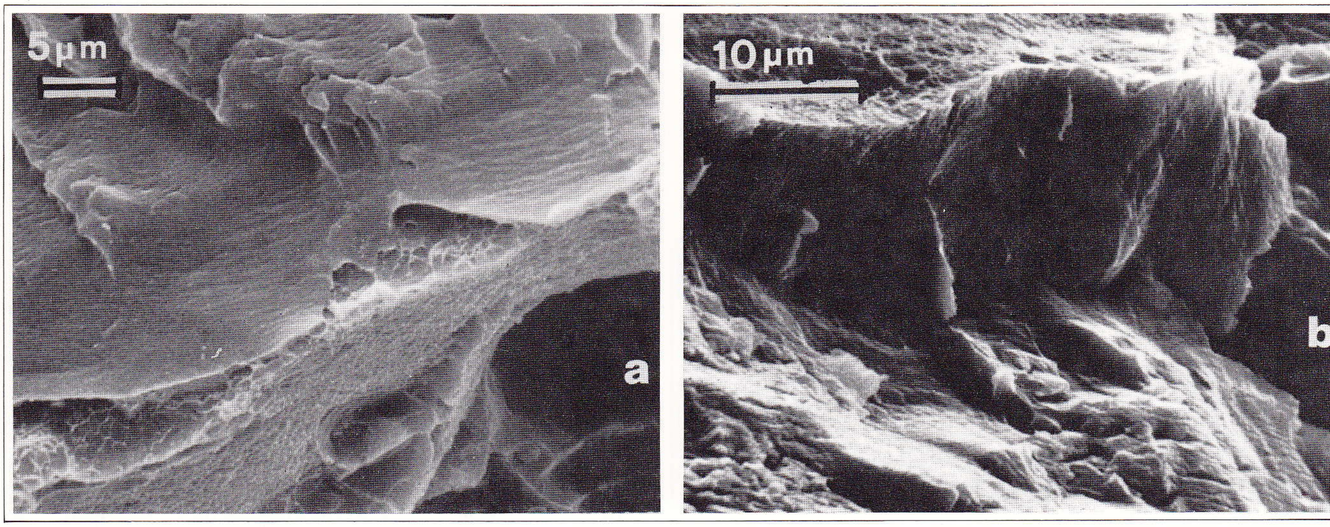

Fig. 9 - Transition region in alloy 2124. The fracture surfaces are explainable as cases (A) and (D) in Fig. 9a and case (B) in Fig. 9b.

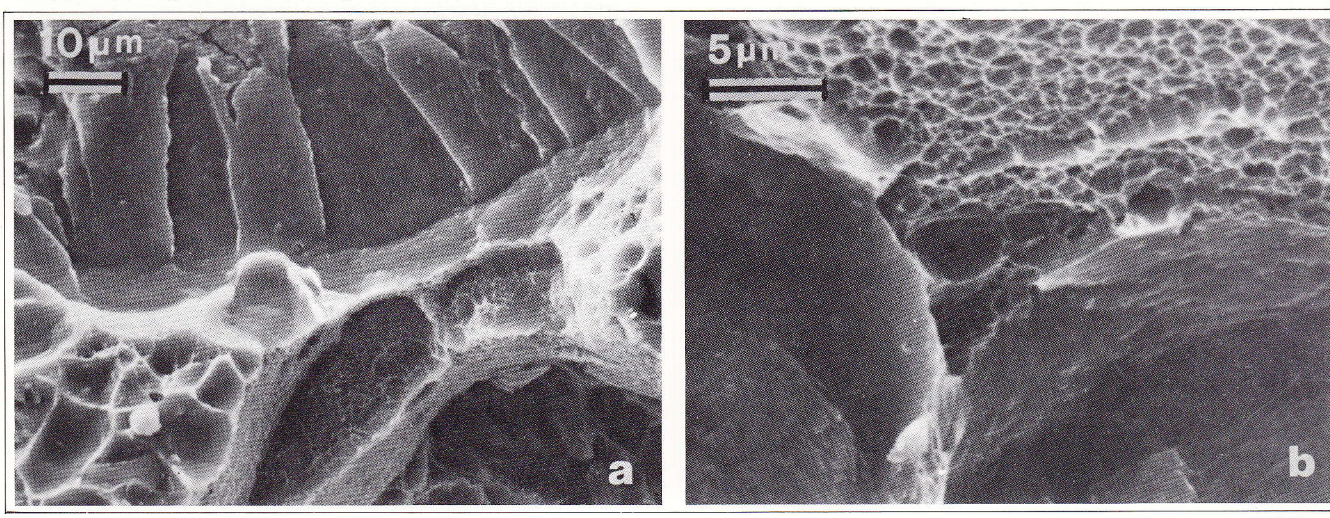

Fig. 10 - Diagrams derived from experimental observations, showing the transition zone and the start of unstable crack propagation.
(A) Probably the most typical case, with cliff present.
(B) No cliff; the first part of the overload fracture is "covered" with microdimples.
(C) Cliff present; unlike case (A) the first part of the overload fracture after the cliff is also "covered" with microdimples.
(D) No cliff; the crack propagates immediately through a region of large dimples.

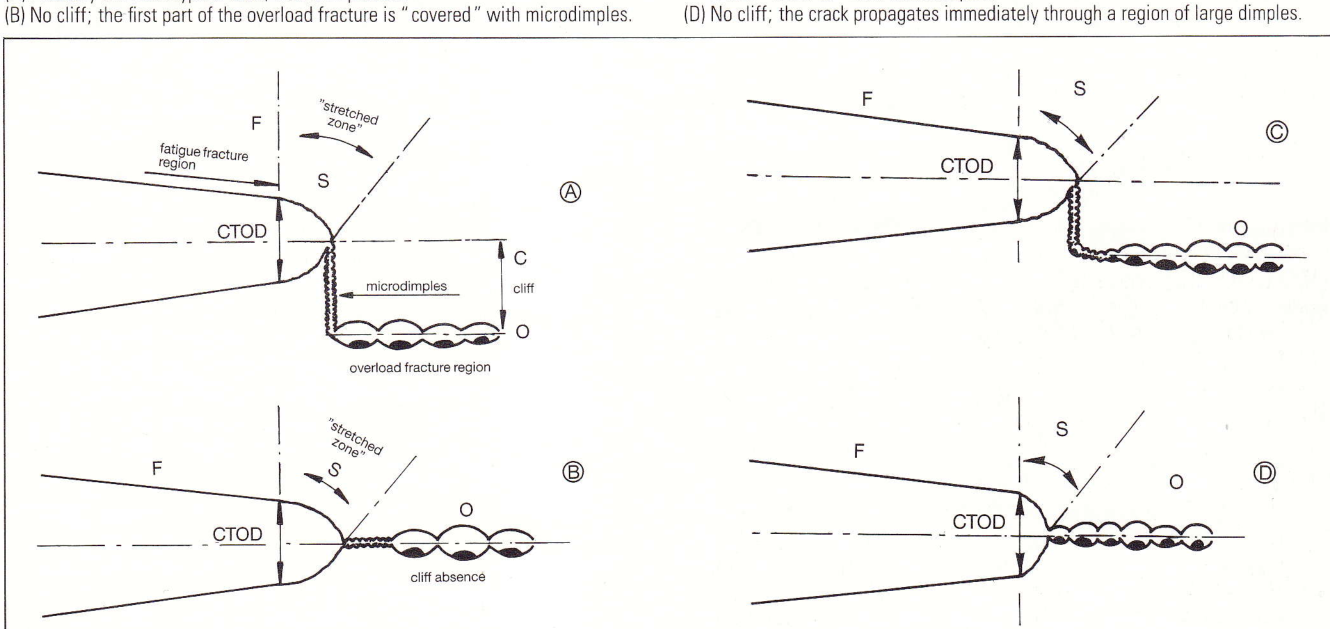

Case C (Fig. 10) - The cliff is still there and microdimples can also be seen in the first part of the overlod fracture zone.
Case D (Fig. 10) - The crack continues in practically the same propagation plane as the fatigue precrack, propagating directly in a series of dimples of varying coarseness.
In Fig. 11 the four cases are compared by plotting the fracture profiles, showing the stretched zone's width W.

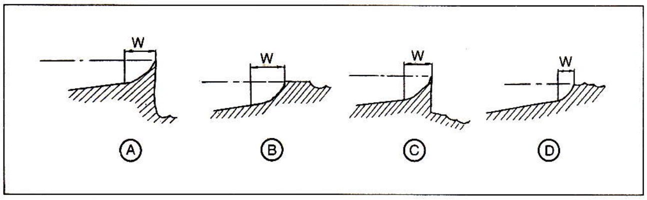

Fig. 11 - Fracture profiles for the cases illustrated in Fig. 10, showing the stretched zone's width W.

Fractographic characteristics and fracture toughness

The attempt to correlate fractographic characteristics with fracture toughness was made by considering the SZ width W, as shown in Fig. 11.
The SZ for each alloy was measured on between 9 and 18 microfractographs at × 500 to × 3000. Several measurements were made on each one, and their average was calculated. These values were used for calculating the average value of W for each alloy.
As has been widely documented, the SZ assumes a curved form; this departs from the mean plane of fatigue crack propagation to varying extents, depending (according to Broek's model) on the blunting of the crack tip, which might reach an opening of 70°.
The measurements made, however, are " linear " readings of what was indicated as the SZ's width W (Fig. 11) and are therefore influenced by the angle of observation, though the error this involves should not result in significant departures from the real values.
Table 3 shows the average values for each micrograph and the average SZ width for each alloy; it can be seen that in few cases the departures from the average exceed 50%.
In calculating the average values no account was taken of nil values, i.e. of the fact that there may be no SZ, particularly for the less tough alloys (2124 and 7050).
In keeping with what was found in the works cited earlier, the results indicate that W_{SZ} increases with increasing K_{Ic}; thus the 7012 alloy has the highest W_{SZ}, followed by alloys 7475, 7010A, 7050 and 2124, in that order.
On the basis of the mechanical and fractographic data described we tried to give an analytic form to the relation between W_{SZ} and K_{Ic}.

TABLE 3 - Average width of stretched zone in each micrograph and for each alloy

Alloy	Average values of W recorded on each micrograph µm	Number of micrographs	Overall average value of W µm	YS N/mm^2	K_{Ic} $N \cdot mm^{-\frac{3}{2}}$	K_{Ic}/YS $mm^{\frac{1}{2}}$
7012 - T7352	17.3 12.9 18.4 14.9 14.6 13.6 24.4 23.7 20.9 18.0 18.0 9.3 35.0	13	18.5	417	985	2.36
7010A - T7352	5.5 6.6 9.3 6.2 7.6 7.9 9.7 7.0 12.0 7.6 6.6 5.7 6.0 8.4 6.2 10.3 4.2 6.4	18	7.4	471	786	1.67
7050 - T73652	5.6 4.4 5.8 8.0 7.3 3.5 6.9 5.2 6.7	9	5.9	484	707	1.46
7475 - T7352	9.0 9.8 8.7 17.3 6.0 7.1 7.3 9.3 5.0 10.0 7.3 11.3	12	9.0	428	871	2.03
2124 - T852	7.9 8.4 4.1 4.0 8.0 1.8 7.0 3.4 8.8 3.3	10	5.7	461	628	1.36

In the same way as Bates et al. (6) and Sarracino and Venzi (11), by analogy with the equation that according to Irwin's model defines the radius of the plastic zone in plane strain conditions, we considered it reasonable that a relation with the following form should be chosen to describe the correlation between W_{SZ} and K_{Ic}:

$$W_{SZ}\ (\mu m) = C\left(\frac{K_{Ic}}{\sigma_{ys}}\right)^{n} \qquad (1)$$

Putting (1) in logarithmic form

$$\left\{\log W_{SZ} = \log C + n\log\left(\frac{K_{Ic}}{\sigma_{ys}}\right)\right\}$$

and applying the least-squares method, in the linear case, we came to the following equation:

$$W_{SZ}\ (\mu m) \approx 2.82\left(\frac{K_{Ic}}{\sigma_{ys}}\right)^{1.97}$$

with a correlation coefficient of 0.94.
Figure 12 plots the values of W_{SZ} versus K_{Ic}/σ_{ys} (0.2) on a logarithmic scale and shows the straight line of interpolation obtained.
In our earlier research (17,18), cliff height measurements led to the equation:

$$h\ (\text{in } \mu m) \approx 2.8\left(\frac{K_{Ic}}{\sigma_{ys}}\right)^{2}$$

which offers an appreciable analogy with what was determined for W_{SZ}.

Possible static fracture model

After studying the different ductile fracture mechanisms proposed by various researchers, including Broek (9), Hahn and Rosenfield (20), Van Stone and Psioda (21), Garrett and Knott (22), Chen and Knott (23), and Firrao and Roberti (14), and in conjunction with our own experimental results, we are able to propose a model of the fracture process at the beginning of unstable crack propagation through overloading that is capable of explaining some of the particular features encountered in the fractographic tests, especially the cliff and its typical orientation in relation to the plane of propagation of the overload fracture.
Before describing the model, we should recall some basic concepts of the process of ductile fracture of high-strength aluminium alloys, particularly the effect of secondary phase particles, dispersoids and so forth, on the material's fracture toughness.
Three types of particles are " active " in relation to fracture behaviour in aluminium alloys of the 7000 and 2000 groups:
a. *Precipitates with a hardening action* of not more than 0.01 µm size consisting of the G.P. zones (pre-precipitates) and transition phases, partly coherent with

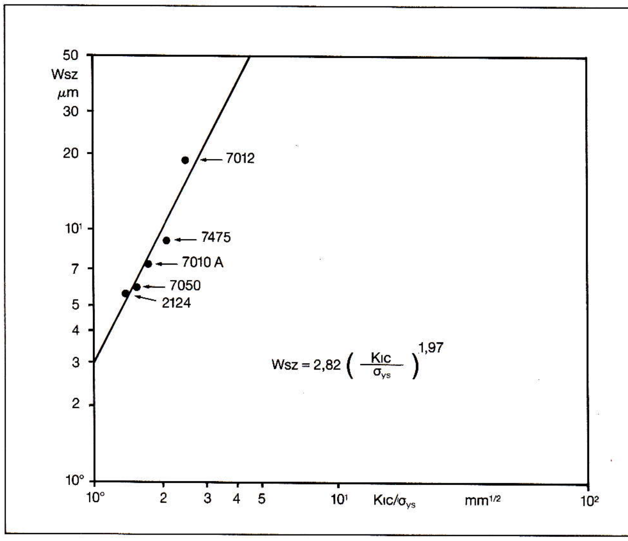

Fig. 12 - Experimental correlation $\log W_{SZ} = \log C + n\log\left(\frac{K_{Ic}}{\sigma_{ys}}\right)$

the matrix, which precede the formation of the equilibrium precipitates, whose size may reach very close to about 0.5 µm.
b. *Particles of intermediate size*, between about 0.03 µm and 0.5 µm (intermediate precipitates or dispersoids), formed during homogenization of the alloy at high temperatures, originating from the three main elements with an antirecrystallizing action: Mn, Cr, Zr.
c. *Coarse particles* (generally indicated as particles of secondary phases), varying in size between about 1 µm and 30 µm, formed during solidification of the alloy or in a subsequent stage by peritectoidic transformation.
It is known that static mechanical fracture in age-hardened high-strength aluminium alloys occurs through the formation of lenticular cavities known as dimples. The dimples that nucleate at intermetallic particles grow and coalesce during deformation.
It is accepted that the dimples originally occur at the coarser particles of secondary phases, which fracture by cleavage under even minor stresses, i.e. through slight strains. The process continues by the nucleation of small dimples at the fine particles (dispersoids and transition precipitates) in the zone of influence of the existing (large) dimples, through fracture of the actual particles, or more probably through their separation from the matrix.
These microdimples coalesce, or join together in laminar assemblies, and bring to the final fracture of the material.
It follows that fracture behaviour is strongly influenced by the density, distribution, size and nature of the finer particles, as well as by the coarse particles.
An increase in the volume fraction of dispersoids (and transition and incoherent particles) involves easier and perhaps faster formation of laminar assemblies of

microdimples, which means a lower resistance to a crack's advance, and therefore, in short, a lower material's toughness. This effect will increase with increasing matrix hardness and will depend on the particles' distribution, their resistance to cleavage, and their interfaces' resistance to separation.
When assessing all the parameters that condition a material's fracture toughness, the above microstructural factors should not be considered without regard to the plastic deformability characteristics of the matrix at the tip of the advancing crack. The admitted amount of local deformation and the volume of material affected by it influence the initiation and growth of the first dimples, but above all they influence the subsequent process in which the dimples are " united " through the formation of microdimples. A tough material is implicitly one in which high plastic deformation occurs before microvoids can nucleate and grow.
If we now consider the typical microstructures of the five alloys and their mechanical properties we can reasonably justify the different fracture toughnesses (in the short transverse direction) obtained on the materials tested.
Alloys 7012 and 7010A present two types of dispersoid, originating from Mn and Zr respectively (24).
The particles containing Zr (globular in form) differ from those containing Mn in that they are partly coherent with the matrix; they are also much smaller ($ZrAl_3$ < 0.03 µm) than the particles of compounds of Mn (+ Fe, + Si) - ($(FeMn)_3 Si_2Al_{15} \geqslant 0.07$ µm).
When it comes to forming microdimples, one particle type will behave differently from the other, and it is reasonable to consider that particles containing Mn will produce microdimple formation " more easily " than those originating from Zr.
The behaviour of Mn dispersoids can be regarded as similar to that of Cr dispersoids (phase E: $Al_{18} Cr_3 Mg_2$: 0.05-1 µm), which also are incoherent with the matrix.

Fig. 13 - Successive stages of the fracture process in plane strain conditions, showing the proposed mechanism of cliff formation. The fracture type is ductile, with formation of laminar assemblies of microvoids.

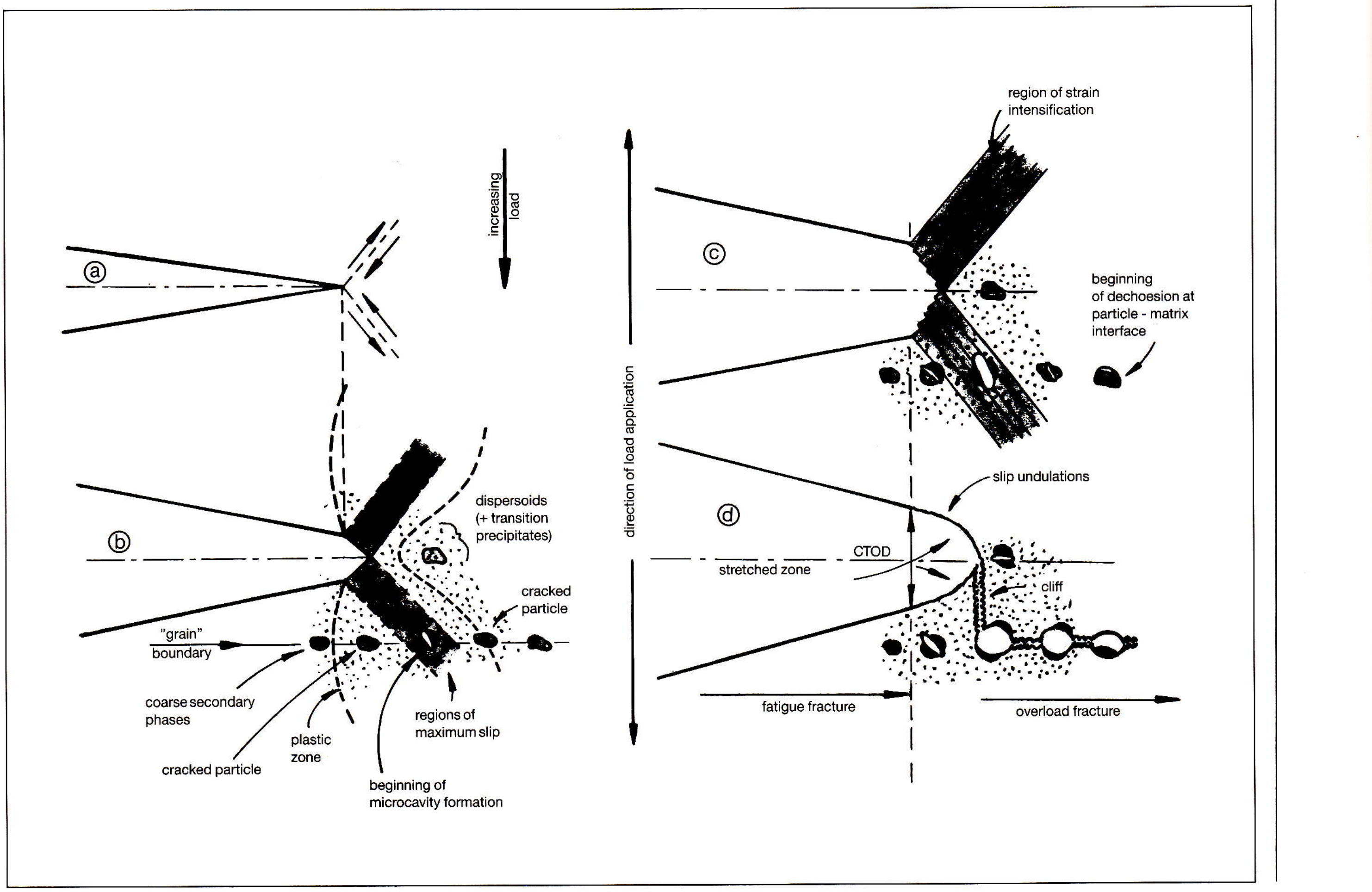

Nevertheless, the density of particles containing Mn in alloys 7012 and 7010A is distinctly lower than the density of particles containing Cr in alloy 7475.
Now let us examine the proposed fracture model, which in plane-strain conditions rests on two fundamental assumptions:
First, the hypothesis put forward by Garrett and Knott (22) and again by Chen and Knott (23), tieing in with a model of the plastic zone proposed by Hahn and Rosenfield (20,25) derived from experimental observations; the hypothesis is that the plastic zone at the crack tip can reasonably be represented as made up of " overlapping regions of shear ".
Second, that inside the plastic zone the process of nucleation and growth of dimples originating at the secondary phase particles will therefore not be homogeneous, so to speak, but will be found to progress more in the " bands " of maximum slip (or maximum shear stress).
Let us consider in detail the sequence of the fracture process according to the diagrams in Fig. 13.
In (a), the fatigue crack in a stress field produces a stress concentration effect at its tip, generating material slip along preferential planes in the directions of maximum shear stress. Following these phenomena, the crack opens, extending its length at the same time, as in (b).
In (b), we see at the crack tip a detail of the plastic zone that precedes it, a zone in which the actual stress exceeds the material's yield strength (the form of the plastic zone is substantially as proposed by various authors).
The two regions of maximum plastic slip can be seen inside the plastic zone.
Growing stress and strain will activate other parallel slip planes, and gradually lead to blunting of the crack tip from (b) to (c).
At the same time as these slip phenomena, the secondary phase particles in positions affected by the plastic strain field that has been created will tend to initiate dimples by fracturing or by separating from the matrix, since they do not have the same deformability as the matrix.
In (b) we also see a few coarse particles, distributed at various distances from the crack tip, inside and outside the plastic zone and more particularly inside and outside the bands of maximum slip.
As explained earlier, at the particles concerned the process of dimple nucleation and growth will be found to progress differently, and the differences in dimple development will remain with the gradual intensification of strain around the crack tip with increasing load, passing from (b) to (c).
In (c), the stepped discontinuities connected with the bands of intense slip at the crack tip are clearly shown.
In (d), the start of unstable propagation of the overload fracture is shown schematically.
The crack will advance along, so to speak, the easiest path. The crack tip will head for the (nearest) larger dimples, through the formation of a laminar assembly of microdimples nucleated around the smaller particles (dispersoids or precipitates). The dispersoids will therefore separate from the matrix when a given critical strain is reached inside the slip bands.
Here in (d) we see the formation of a cliff at an angle of just about 90° to the plane of propagation of the overload fracture. The formation and orientation of the cliff, which as explained is covered with small dimples, are explained by the crack tip's " need " to " unite " with the series of larger dimples lying, in the present case, in a lower plane.
The laminar assembly must be regarded as originating under such high local stress and strain as to entail the growth and immediate coalescence of its constituent microdimples. More correctly, it must be accepted that coalescence occurs immediately after the voids are formed by decohesion because no appreciable distorsion is detected in the shape of the microvoids on the cliff walls.
The stretched zone, on the other hand, appears as deriving from the tip blunting process and thus is closely correlated with the CTOD.
So, as can be seen from the sequence in Fig. 13, the cliff, if any, tends to assume directions roughly normal to the crack's mean propagation plane, and to go " up " or " down " to join the most suitable overload fracture propagation plane. There may even be no cliff, if propagation happens to be " easiest " in the same plane as the fatigue fracture, for if the crack tip involves a " grain " boundary or a row of particles it is evident that the crack will subsequently advance without appreciable deviations, as illustrated in diagrams B and D of Fig. 10 and 11.

Conclusions

The fundamental purpose of our work was to find a correlation between the microfractographic characteristics and the fracture toughness data recorded on a number of CT test pieces of five high-strength alloys of the 7000 and 2000 series.
A relation was formulated, in a form suggested by the theories of fracture mechanics; it links the average widths of the stretched zone for the five alloys with their K_{Ic} values, interpolating the experimental data with adequate accuracy.
In addition, on the basis of SEM observations and the existing literature on the subject, it was possible to propose a plausible static fracture model that gives a reasonable explanation of the micromechanisms underlying the formation of the SZ and the cliff in

particular, and the triggering of fast fracture through overload in general.
We should once again emphasize the importance assumed by the interpretation of these fracture surface characteristics as experimental verification of the rupture mechanisms and therefore of the mechanical and microstructural characteristics of a material.

REFERENCES

(1) I.S.M.L. Indagini su leghe sperimentali da fucinatura del sistema AL-Zn-Mg-Cu (−Zr). Relazione finale. Contratto AM 116 n° 3563 di repertorio. ***Rapporto ISML 78/24 878*** *(1978).*

(2) Spitzig, W.A. A fractographic feature of plane-strain fracture in 0,45 C-Ni-Cr-Mo steel. ***Trans. ASM, 61*** *(1968), 344-349.*

(3) Krafft, J.M. Correlation of plane strain crack toughness with strain hardening characteristics of a low, a medium, and a high strength steel. ***Appl. Mater. Res., 3(2)*** *(1964), 88-101.*

(4) Krafft, J.M. Dynamic mechanical behaviour of metal at the tip of a plane-strain crack. Pre. at ***S.W. Int. Symp. on Dynamic Loading,*** *San Antonio, 1967.*

(5) Spitzig, W.A. Correlation between fractographic features and plane-strain fracture toughness in an ultrahigh-strength steel. In ***Electron Microfractography. ASTM STP 453****. American Society for Testing and Materials, Philadelphia, 1969, pp. 90-110.*

(6) Bates, R.C., W.G. Clark, and D.M. Moon. Correlation of fractographic features with fracture mechanics data. In ***Electron Microfractography. ASTM STP 453.*** *American Society for Testing and Materials, Philadelphia, 1969, pp. 192-214.*

(7) Otsuka, A., T. Miyata, S. Nishimura, and Y. Kashiwagi. ***Engineering Fracture Mechanics, 7*** *(1975), 419-428.*

(8) Gerberich, W.W., and P.L. Hemmings. Fractographic observations of stretched regions in front of fatigue cracks, ***Trans. ASM, 62*** *(1969), 540-543.*

(9) Broek, D. Correlation between stretched zone size and fracture toughness. ***Eng. Fract. Mech., 6*** *(1974), 173-181.*

(10) Krasowsky, A.J., and V.A. Vainshtok. On a relationship between stretched zone parameters and fracture toughness of ductile structural steels. ***Int. J. Fract., 17*** *(1981), 579-592.*

(11) Sarracino, M., and S. Venzi. Possibilità di correlazione fra i risultati dell'esame microfrattografico e le proprietà di tenacità alla frattura di un acciaio da bonifica. ***Metall. Ital., 66*** *(1974), 14-20.*

(12) McClintock, F.A., and G.R. Irwin. ***Plasticity Aspects of Fracture Mechanisms. ASTM STP 381.*** *American Society for Testing and Materials, Philadelphia, 1965, pp. 84-113.*

(13) Firrao, D., and R. Roberti. A model for plane strain ductile fracture toughness. In R.C. Gifkins (Ed.) ***Strength of Metals and Alloys.*** *Pergamon Press, Oxford, 1982, pp. 947-952.*

(14) Firrao, D., and R. Roberti. Ductile fracture nucleation ahead of sharp cracks. ***Metallurgical Science and Technology, 1*** *(1983), 5-13.*

(15) Firrao, D., and R. Roberti. Sui parametri microstrutturali che controllano la tenacità alla frattura degli acciai. ***Metall. It., 75*** *(1983), 645-651.*

(16) Peel, C.J., R.N. Wilson, and P.J.E. Forsyth. Relationships between some microstructural features and the fracture toughness of an Al-Zn-Mg-Cu-Mn forging alloy. ***Metal Sci. J., 6*** *(1972), 102-106.*

(17) Di Russo, E., G. Oddone, F. Gatto, and M. Buratti. Caratteristiche frattografiche e tenacità alla frattura di leghe Al-Zn-Mg-Cu-Zr. ***Alluminio, 43*** *(1974), 415-430.*

(18) Di Russo, E., M. Buratti, A. Giarda, and G. Oddone. The effect of the grain and precipitation structures on ductility and fracture toughness of Al-Zn-Mg-Cu-Cr alloys. In ***VI Internationale Leichtmetalltagung****, Leoben-Wien, 1975. Aluminium-Verlag, Duesseldorf, 1975, pp. 36-39.*

(19) Broek, D. The role of inclusions in ductile fracture and fracture toughness. ***Eng. Fract. Mech., 5(1)*** *(1973), 55-66.*

(20) Hahn, G.T., and A.R. Rosenfield. Metallurgical factors affecting fracture toughness of aluminum alloys. ***Metall. Trans. A, 6A*** *(1975), 653-668.*

(21) Van Stone, R.H., and J.A. Psioda. Discussion of metallurgical factors affecting fracture toughness of aluminum alloys. ***Metall. Trans. A. 6A*** *(1975), 668-670.*

(22) Garrett, G.G., and J.F. Knott. The influence compositional and microstructural variations on the mechanism of static fracture in aluminum alloys. ***Metall. Trans. A, 9A*** *(1978), 1187-1201.*

(23) Chen, C.Q., and J.F. Knott. Effect of dispersoid particles on toughness of high-strenth aluminum alloys. ***Met. Sci., 15*** *(1981); 357-364.*

(24) Buratti, M., and E. Di Russo. Fasi secondarie, strutture di precipitazione e tenacità di leghe 7000 ad elevata resistenza. ***Alluminio, 49*** *(1979), 31-46.*

(25) Hahn, G.T., and A.R. Rosenfield. Sources of fracture toughness: the relation between K_{Ic} and the ordinary tensile properties of metals. In ***Application-related Phenomena in Titanium Alloys. ASTM STP 432,*** *American Society for Testing and Materials, Philadelphia, 1968, pp. 5-32.*